Research article

NMR IN BIOMEDICINE

Received: 22 July 2014, Revised: 12 November 2014, Accepted: 3 December 2014, Published online in Wiley Online Library

(wileyonlinelibrary.com) DOI: 10.1002/nbm.3254

^{1}H NMR spectroscopy of glioblastoma stem-like cells identifies alpha-aminoadipate as a marker of tumor aggressiveness

Antonella Rosi[a,b]*†, Lucia Ricci-Vitiani[c†], Mauro Biffoni[c], Sveva Grande[a,b], Anna Maria Luciani[a,b], Alessandra Palma[a,b], Daniele Runci[c], Marianna Cappellari[c], Ruggero De Maria[d], Laura Guidoni[b‡], Roberto Pallini[e‡] and Vincenza Viti[b‡]

Patients suffering from glioblastoma multiforme (GBM) face a poor prognosis with median survival of about 14 months. High recurrence rate and failure of conventional treatments are attributed to the presence of GBM cells with stem-like properties (GSCs). Metabolite profiles of 42 GSC lines established from the tumor tissue of adult GBM patients were screened with ^{1}H NMR spectroscopy and compared with human neural progenitor cells from human adult olfactory bulb (OB-NPCs) and from the developing human brain (HNPCs).

A first subset ($n = 12$) of GSCs exhibited a dramatic accumulation of the metabolite α-aminoadipate (αAAD), product of the oxidation of α-aminoadipic semialdehyde catalyzed by the ALDH7A1 aldehyde dehydrogenase (ALDH) family in lysine catabolism. αAAD was low/not detectable in a second GSC subset ($n = 13$) with the same neural metabolic profile as well as in a third GSC subset ($n = 17$) characterized by intense lipid signals. Likewise, αAAD was not detected in the spectra of OB-NPCs or HNPCs. Inhibition of mitochondrial ATP synthase by oligomycin treatment revealed that the lysine degradative pathway leading to αAAD formation proceeds through saccharopine, as usually observed in developing brain. Survival curves indicated that high αAAD levels in GSCs significantly correlated with poor patient survival, similarly to prostate and non-small-cell-lung cancers, where activity of ALDH7A1 correlates with tumor aggressiveness. **Copyright © 2015 John Wiley & Sons, Ltd.**

Additional supporting information may be found in the online version of this article at the publisher's web site.

Keywords: glioblastoma stem-like cells; ^{1}H NMR spectroscopy; alpha aminoadipate; lipids; patient survival

INTRODUCTION

Glioblastoma multiforme (GBM) is very difficult to treat and patients face a poor prognosis, with a median survival of about 14 months (1). High recurrence rate and failure of conventional treatments are attributed to the presence of GBM cells with stem-like properties (glioblastoma stem-like cells, GSCs).

The members of the aldehyde dehydrogenase (ALDH) gene superfamily (2) have been considered as a possible marker of tumor stemness (3).

The ALDH superfamily is composed of nicotinamide adenine dinucleotide phosphate-dependent enzymes that catalyze the oxidation of aldehydes to their corresponding carboxylic acids. To date, 19 ALDH gene families have been identified in the eukaryotic genome (4) that are also found in stem cells (3). In particular, the isoform ALDH7A1, also known as antiquitin, is implicated in lysine (Lys) catabolism in humans, progressing in a sequence of seven reactions that leads to the fatty acid pathway. The first step of Lys degradation occurs either by

* *Correspondence to: Antonella Rosi, Department of Technology and Health, Istituto Superiore di Sanità, Rome, Italy. E-mail: antonella.rosi@iss.it*

a *A. Rosi, S. Grande, A. M. Luciani, A. Palma*
Department of Technology and Health, Istituto Superiore di Sanità, Rome, Italy

b *A. Rosi, S. Grande, A. M. Luciani, A. Palma, L. Guidoni, V. Viti*
INFN Sezione di Roma, Rome, Italy

c *L. Ricci-Vitiani, M. Biffoni, D. Runci, M. Cappellari*
Department of Hematology, Oncology and Molecular Medicine, Istituto Superiore di Sanità, Rome, Italy

d *R. De Maria*
Regina Elena National Cancer Institute, Rome, Italy

e *R. Pallini*
Department of Neurosurgery, Università Cattolica del Sacro Cuore, Rome, Italy

† *These two authors equally contributed to the manuscript.*

‡ *These authors share senior authorship.*

Abbreviations used: *GBM, glioblastoma multiforme; GSCs, glioblastoma stem-like cells; ALDH, aldehyde dehydrogenase; αAAD, α-aminoadipate; HNPCs, human neural progenitor cells; OB-NPCs, olfactory bulb neural progenitor cells; CSF, cerebrospinal fluid; MGMT, O6-methylguanine-DNA methyltransferase; PCR, polymerase chain reaction; TMSP, sodium 3-(trimethyl-silyl) propionate 2,2,3,3-d; PCA, perchloric acid; COSY, correlation spectroscopy; ML, mobile lipids; GABA, γ-amino-butyric acid; KPS, Karnofsky performance status; OS, overall survival; PFS, progression-free survival; 2-AAT, 2-aminoadipate aminotransferase.*

Copyright © 2015 John Wiley & Sons, Ltd.

mitochondrial ε-deamination in the saccharopine pathway or by peroxisomal α-deamination in the pipecolic acid pathway. The saccharopine pathway is active in the fetal brain while the pipecolic pathway is active in the adult brain (5). Both pathways converge to formation of α-aminoadipic semialdehyde, which is further oxidized to α-aminoadipate (αAAD), a reaction catalyzed by ALDH7A1.

αAAD is present in human brain (6) and in human cerebrospinal fluid (CSF) at a low concentrations (micromolar) (7,8). This metabolite has never been detected in NMR spectra from neural cells *in vitro* (9) or from mammalian brain *in vivo* even at very high magnetic fields (10), as its low concentration is below the NMR detection limit. αAAD levels were found to be significantly increased in the CSF of glioma patients (11). Furthermore, analysis of metabolites secreted and consumed by cancer cells identified αAAD as a potential biomarker of cancer (12). More recently, αAAD has been detected by mass spectrometry in surgery-derived glioma tissues (13).

Here, we report for the first time the detection of a new signal in NMR spectra of GBM deriving cells, attributed to αAAD. The Lys catabolic pathway started from the mitochondrial saccharopine step, as usually observed in developing brain. A dramatic accumulation of αAAD was observed in a subset of 12 GSC lines deriving from a cohort of 42 GBM patients. An inverse relationship was found between αAAD signal levels in GSCs and patient survival, suggesting a role for αAAD as a novel prognostic factor in GBM tumors.

MATERIALS AND METHODS

Enrollment of patients, diagnosis, and tumor characterization

Tumor tissue samples were harvested from 42 patients undergoing craniotomy at the Institute of Neurosurgery, Catholic University School of Medicine, Rome, Italy. All the patients provided written informed consent according to the research proposals approved by the Ethical Committee of the Catholic University School of Medicine. Patients were eligible for the study if a diagnosis of GBM was established histologically according to the WHO classification.

After surgery, the treatment plan included radiotherapy concomitant temozolomide for 7 d a week from the first to the last day of radiotherapy followed by five cycles of adjuvant temozolomide given at 4 week intervals. Survival was calculated from the date of surgery. The disease was considered to have progressed if both the diameter and volume of the tumor increased by 25% of initial measurements or more, if a new lesion was evident on an axial contrast-enhanced T_1-weighted MRI scan, or if the patient's neurologic condition worsened and required an increased dose of steroids.

O6-methylguanine-DNA methyltransferase (MGMT) promoter methylation patterns were studied by methylation-specific polymerase chain reaction (PCR) using primers specific for methylated and unmethylated DNA on genomic DNA extracted from paraffin-embedded tissue using a QIAamp DNA Mini Kit (Qiagen Venlo, Linburgo, Netherlands). The annealing temperature was 60 °C. DNA from normal lymphocytes treated with SssI methyltransferase (New England Biolabs, Ipswich, Massachusetts, USA) was used as a positive control for methylated and unmethylated alleles of MGMT. PCR products were separated onto 3% agarose gel, stained with ethidium bromide, and visualized under UV illumination.

GSC isolation and treatment

GSC lines were isolated through mechanical dissociation of the tumor tissue and cultured in a serum-free medium supplemented with EGF and basic FGF as described (14); the neural origin of cultured cells was assessed by phenotypic and functional characterization (15). Olfactory bulb neural progenitor cells (OB-NPCs) were isolated from surgical specimens as previously described (16,17). Neural progenitor cells derived from the developing human brain, HNPCs, were purchased from Lonza (Basel, Switzerland).

For the evaluation of oligomycin effects on GSC metabolism and proliferation, cells were plated at a density of 2×10^4/ml in 96-well plates in triplicate, or in 75 mm^3 flasks, and incubated at 37 °C in a 5% CO_2 atmosphere. After one week of culture cells were treated for 24 h with 1 μM oligomycin in culture medium. Cell proliferation was monitored by counting the cells and confirmed using the CellTiter-Blue Cell Viability Assay. For NMR samples exponentially growing cells were treated in fresh medium with 1 μM oligomycin for 7.5 and 24 h and then prepared for NMR experiments.

^{1}H NMR sample preparation

GSCs were washed in PBS and centrifuged at 162 relative centrifugal force (RCF) for 3 min. The pellet of about 2×10^6 cells was suspended in PBS with 20% D_2O and 2 mM sodium 3-(trimethyl-silyl) propionate 2,2,3,3-d (TMSP) as a frequency standard. An aliquot (volume 15 μl) of the suspension was inserted in a 1 mm NMR tube and then centrifuged to obtain the final packed cell volume; all cell samples were within the sensible NMR coil volume. Perchloric acid (PCA) extracts were prepared as described in a previous work (18). 10 mM L2-aminoadipic acid pure compound was dissolved in H_2O with 2 mM TMSP and 10% D_2O, at pH 7. All NMR reagents were purchased from Cambridge Isotope Laboratories (Cambridge, UK).

^{1}H NMR measurements

1D and 2D correlation spectroscopy (COSY) ^{1}H NMR experiments were run at 400.14 MHz and at $T = 298$ K on a digital Bruker Avance spectrometer equipped with a 1 mm microprobe.

NMR measurements and spectral analysis were performed as previously described (18,19). In particular, 1D ^{1}H NMR spectra were acquired with a 90° RF pulse. Intact cell spectra were acquired with a number of scans (n_s) equal to 1000 (sufficient to

Table 1. Patient data of the cohort of $n = 42$ patients (n is total including censored). 4.0 and 10.5 months are the medians of the progression-free survival (PFS) and OS respectively

	Patient data	Number of patients
Age (years)	<70	21
	>70	21
Gender	F	10
	M	32
KPS (%)	<70	28
	>70	14
PFS (months)	>4.0	21
	<4.0	21
OS (months)	>10.5	22
	>10.5	20

Copyright © 2015 John Wiley & Sons, Ltd.

obtain a good signal-to-noise ratio), while $n_s = 4000$ was used for PCA extract and culture media spectra. 2D COSY spectra were acquired with a 90°–t_1–90°–t_2 pulse sequence and $n_s = 32$ for cell or $n_s = 128$ for PCA extracts and culture media samples. Spectra were acquired as a matrix of 512×128 data points in the time domain. A Lorentzian–Gaussian function was applied, when indicated, in the time domain before Fourier transformation. Chemical shifts were measured with respect to Lac methyl signal at 1.33 ppm in 1D and to lactate cross peak at 1.33–4.12 ppm in 2D COSY cell spectra. Water suppression in 1D and 2D experiments was obtained using presaturation spectra. The measurement of cell samples lasted approximately 210 min (60 min for the 1D experiment and 150 min for the 2D experiment). Cell viability, tested by the trypan blue exclusion method, was greater than 90% at the beginning of the preparation and greater than 80% at the end of the NMR measurements, in agreement with previous works (18,19). NMR parameters were obtained in at least three independent experiments and data are expressed as mean ± standard deviation (SD) values.

2D COSY spectroscopy provided spectral assignment opportunities with off-diagonal elements giving information on metabolite concentrations. As the presence of the mobile lipid (ML)

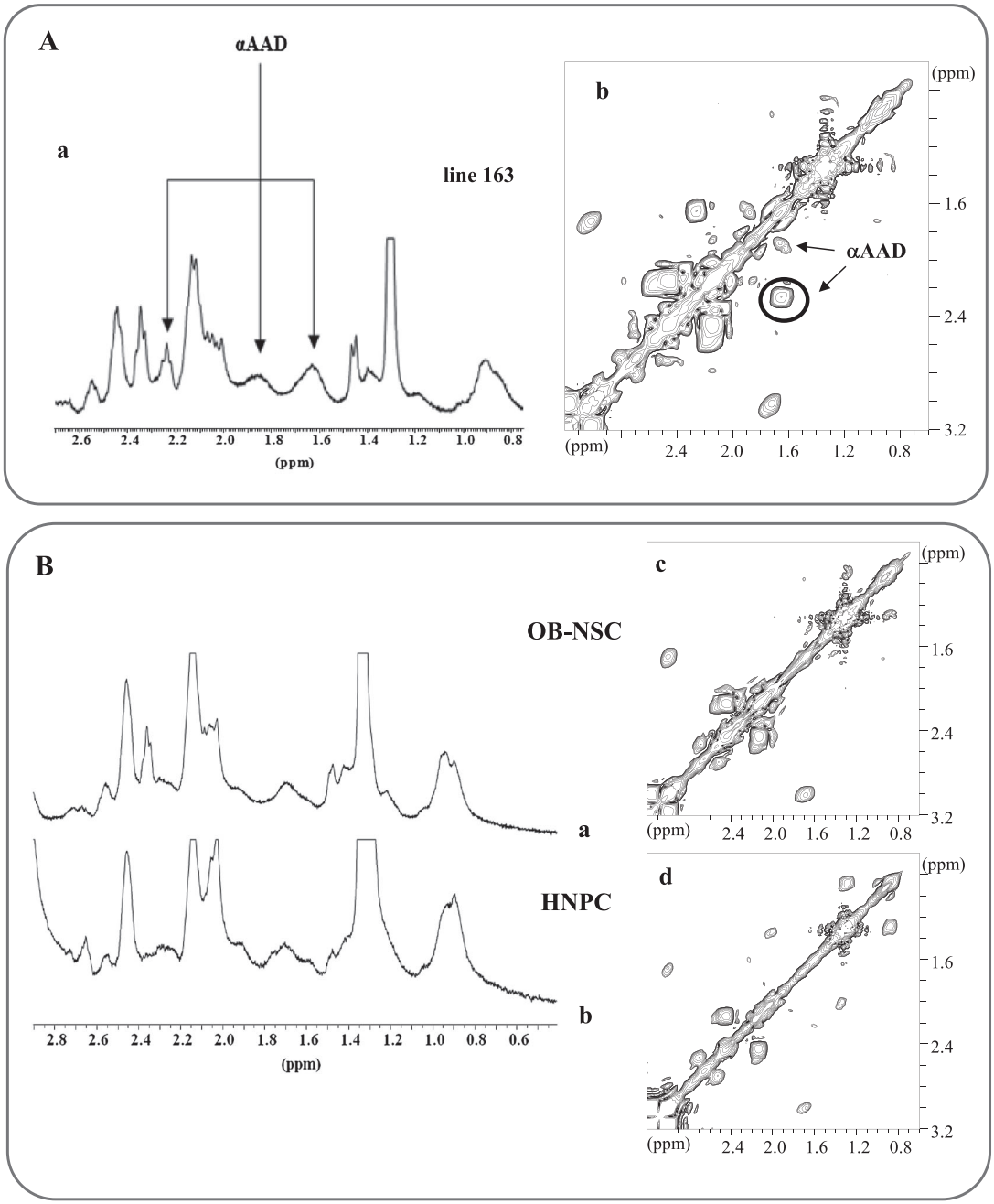

Figure 1. 1D and 2D COSY spectra (high field region) of line 163 (A)(a), (b), of a line from human adult OB-NPC cells (B)(a), (c) and of a line from HNPC cells derived from the developing human brain (B)(b), (d). Spectra of line 163 show the new signals at 2.26 in 1D (A)(a) and the two relative cross peaks at 2.25–1.65 ppm and 1.87–1.65 ppm in 2D COSY spectra (A)(b) discussed in the text.

Copyright © 2015 John Wiley & Sons, Ltd.

signals often hindered a reliable intensity measurement in the 1D spectra, 2D COSY was preferentially used for a quantitative evaluation of signal intensities. The 1D spectra were utilized to confirm the general trends of NMR signal intensities. 2D WIN-NMR software (Bruker, AG, Darmstadt, Germany) was used to perform cross peak integration.

Table 2. αAAD signal assignments in spectra of αAAD pure compound, GSC line 163, and PCA extracts from line 163

	1D peaks (ppm)		
Proton	αAAD molecule	Cells – line163	PCA – line163
H2	3.743 (dd)	crowded	crowded
H3 (H3′)	1.860 (m)	1.86 (m)	1.861 (m)
H4 (H4′)	1.641 (m)	1.65 (m)	1.652 (m)
H5 (H5′)	2.251 (t)	2.25 (t)	2.250 (t)
		2D COSY cross peaks (ppm)	
Proton	αAAD molecule	Cells – line163	PCA – line163
H3(H3′)–H2	1.85–3.73	1.87–3.75	1.85–3.77
H4 (H4′)–H3 (H3′)	1.63–1.85	1.66–1.89	1.64–1.85
H4 (H4′)–H5 (H5′)	1.64–2.25	1.66–2.26	1.64–2.24

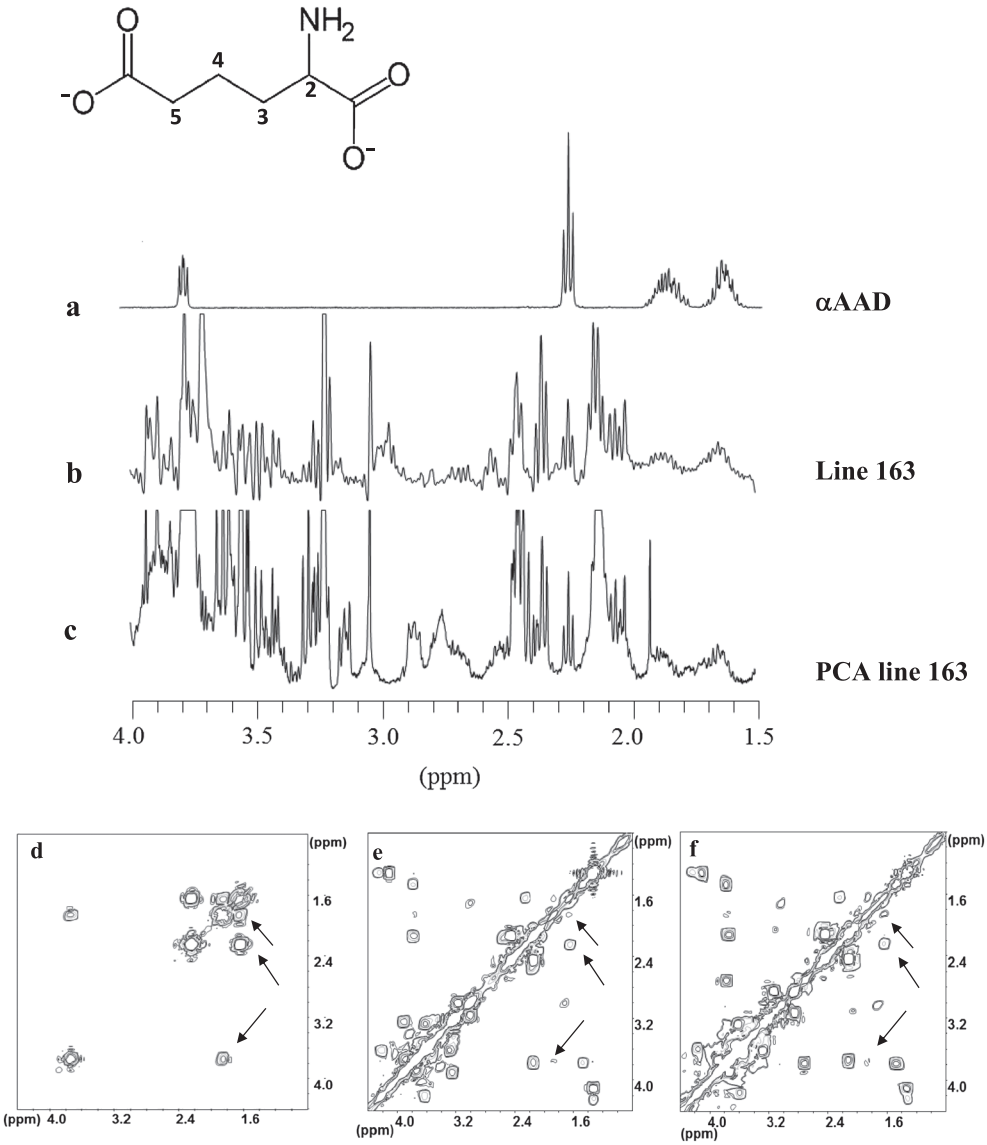

Figure 2. Signals in 1D and 2D COSY spectra (high field region) of αAAD pure compound in solution (a), (d), in line 163 (b), (e), and in relative PCA extracts (c), (f). The structure of the αAAD molecule is also shown. A Lorentzian–Gaussian function (LB = −10, GB = 15) was applied in the time domain before Fourier transformation for signals of trace (b). Arrows indicate signals common to all 2D COSY spectra.

Copyright © 2015 John Wiley & Sons, Ltd.

The size of each rectangle marking the area used for volume integration of 2D COSY cross peaks was optimized according to previous studies (19,20), covering the peak and avoiding superimposing neighboring peaks. After a few spectrum evaluations, optimized rectangle sizes (areas of integration) were determined and applied to all spectra. The plane baseline was evaluated and subtracted from the integrals. In the region close to the main diagonal of 2D spectra, the baseline was slightly higher, as already observed in brain spectra (20). This may give a small intensity contribution even when a cross peak is not observed.

ML signal integrals were normalized to the intensity of the Lys cross peak at 1.70–3.00 ppm, as indicated in the legend of Figure 5(a). This peak was considered representative of the cellular mass according to Palma *et al*. (18) and references therein. αAAD being derived from Lys, the intensity ratio αAAD/(αAAD + Lys), which gives the percentage of catabolized Lys, was monitored when groups of different αAAD intensity were considered, as indicated in the legend of Figure 5(b).

Statistical analysis

Survival curves were generated using the Kaplan–Meier method. Multivariate analysis for patient survival was performed using the Cox proportional hazard model. All *p*-values are based on two-tailed tests and differences were considered statistically significant when $p < 0.05$. The statistical software StatView 5.0 (SAS Institute, Cary, NC, USA) was used for statistical analysis.

RESULTS

Intense peaks in ^{1}H NMR spectra from GSC identify αAAD

The metabolic profiles of 42 GSC lines were analyzed by ^{1}H NMR spectroscopy during exponential growth. Patients' characteristics are reported in Table 1. NMR spectra were run from intact cells and compared, when necessary, to those from PCA extracts. Cell spectra provided information that could not be obtained from PCA extracts, e.g. ML signals.

Exponentially growing cells showed a very active metabolism, as previously described (19). Spectra were characterized by the neural markers myoinositol and N-acetylaspartate and by many signals observed in glioma and in neural cells, such as creatine, glutamine, and aspartate (19). A group of 17 out of 42 GSC lines displayed spectra with intense signals from ML, mainly triglycerides. Conversely, the spectra of the other 25 GSC lines had low or not-detectable ML signals during exponential growth, which increased close to cell proliferative arrest with a behavior shared by tumor cells of different histologies (19,21,22).

Three signals at 2.25, 1.86, and 1.65 ppm appeared in 1D ^{1}H NMR spectra of 25 GSC lines (Fig. 1(A)(a)). In parallel, 2D COSY ^{1}H NMR spectra of the same GSCs showed two cross peaks at

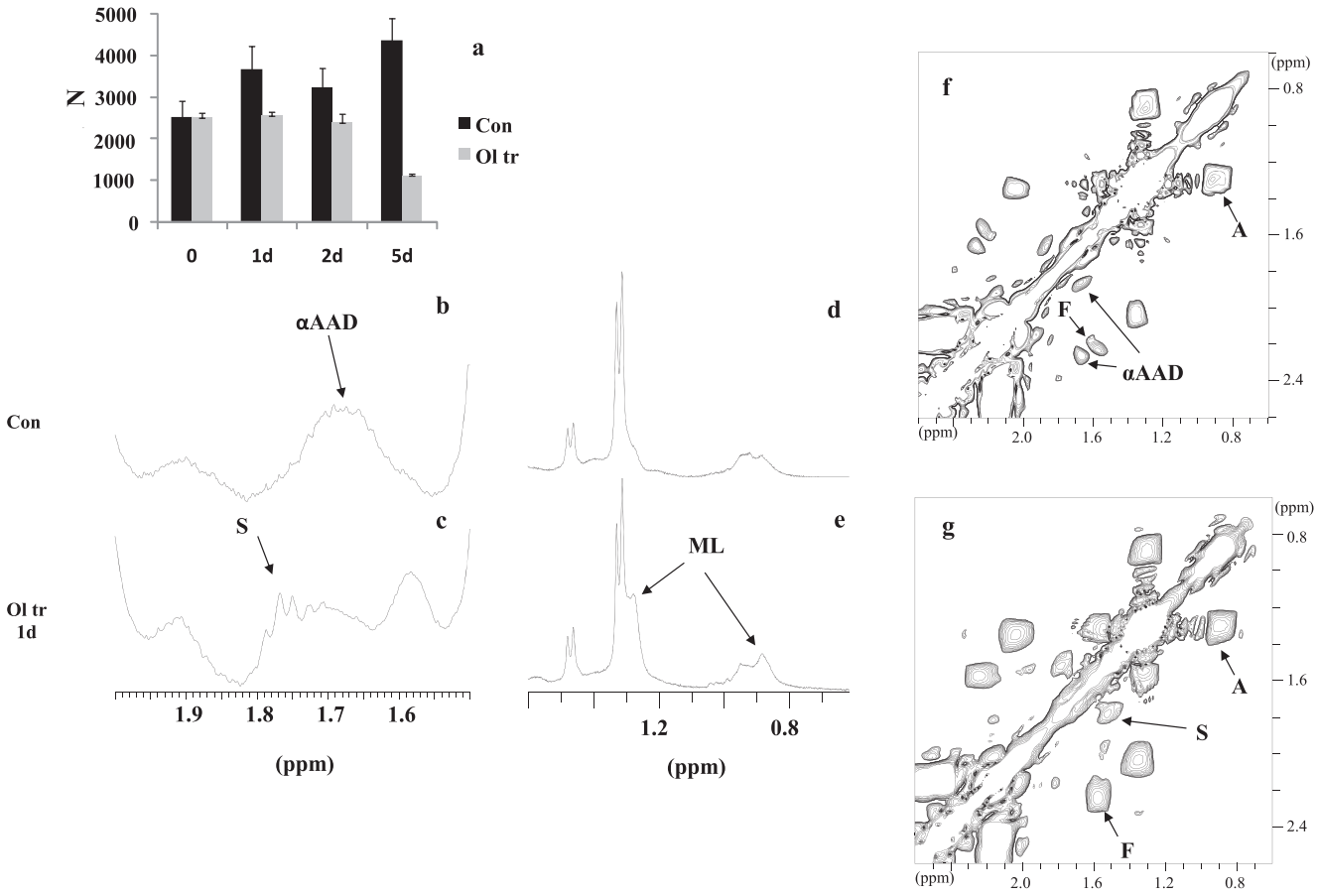

Figure 3. (a) Line 163 cell viability through CellTiter-Blue Cell Viability Assay for control (con) and oligomycin treated (ol tr) cells. *N* is the cell number at different days *d* after treatment. (b)–(g) 1D and 2D COSY spectra of untreated and 24 h oligomycin treated cells from line 163. S stands for saccharopine. Cross peak A is from terminal methyl and bulk methylene protons and cross peak F from methylene protons at C3 and C2 in fatty acid.

Copyright © 2015 John Wiley & Sons, Ltd.

2.25–1.65 ppm and 1.87–1.65 ppm (Fig. 1(A)(b)), whose intensities were related to 1D signal intensities. These signals were not detectable in the spectra of OB-NPCs (Fig. 1(B)(a), (c)) and HNPCs (Fig. 1(B)(b), (d)), where ML signals were present at low intensity as expected in these cells when actively proliferating (23).

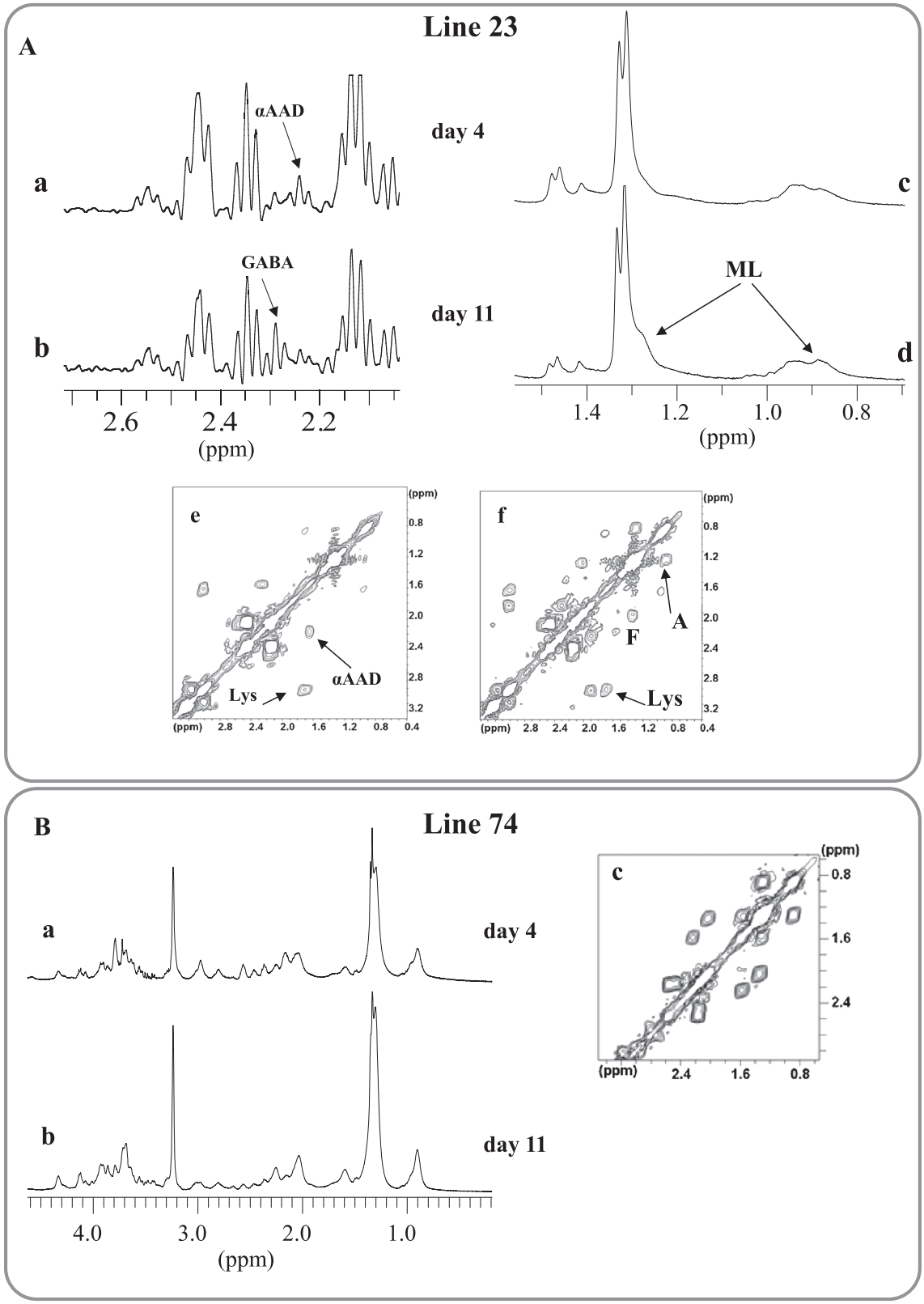

Figure 4. (A) 1D and 2D COSY spectra of line 23 at day 4 (a), (c), (e) and at day 11 (b), (d), (f) after seeding. (B) 1D and 2D COSY spectra of line 74 at day 4 (a), (c) and at day 11 (b) after seeding. A Lorentzian–Gaussian function (LB = −10, GB = 15) was applied in the time domain before Fourier transformation for signals of traces (A)(a), (b).

Copyright © 2015 John Wiley & Sons, Ltd.

Assignment of these signals to αAAD molecule (Table 2) was possible on the basis of the full analysis of 1D and 2D spectral pattern of intact GSCs (Fig. 2(b), (e)) and their PCA extracts (Fig. 2 (c), (f)) and the comparison with the pure compound spectra (Fig. 2(a), (d)). As shown in Figure 2(a) and according to current literature (24), the αAAD molecule has five non-exchangeable scalar-coupled protons giving rise to a doublet of doublets (H2) resonating at 3.74 ppm, a multiplet (H3 and H3′) at approximately 1.83 ppm, a multiplet (H4 and H4′) at approximately 1.65 ppm, and a triplet (H5 and H5′) at 2.25 ppm ($J = 7.4$ Hz). Figure 2(d) shows the 2D COSY spectra of the αAAD pure compound, with the cross peaks at 1.83–1.65 ppm, at 1.65–2.25 ppm, and, less intense, at 3.73–1.83 ppm. The spectrum of Figure 2(b) is from the exemplificative GSC line, namely line 163, characterized by intense signals at 2.25, 1.86, and 1.65 ppm. Apodization with a Lorentzian–Gaussian function shows that the signal at 2.25 is a triplet while the other two signals are multiplets (Fig. 2(b)). The triplet has coupling constant $J = 7.34$ Hz. The field region around 3.7 ppm is very crowded, with signals overlapping precluding signal identification in 1D cell spectra; in the 2D COSY spectrum (Fig. 2(e)) a cross peak at 3.74–1.85 ppm with a lower intensity is visible. Besides, coupling of the signal at 2.25 ppm with the peak at 1.65 ppm, which is also coupled with the peak at 1.85 ppm, was observed. The same signal pattern is visible in 1D and 2D spectra of PCA extracts of the same cells, as shown in Figure 2(c), (f). Spiking with the pure αAAD compound was also performed (not shown).

The cross peak at 2.25–1.65 ppm is specific to αAAD, allowing us to discriminate it from other molecules with similar structures. Glutaric acid has a triplet at 2.17 ppm in 1D spectra, but the cross peak is at 2.17–1.77 ppm; hydroxyglutaric acid has a multiplet at 2.25 ppm, but the cross peak is at 2.25–1.90 ppm; γ-amino-

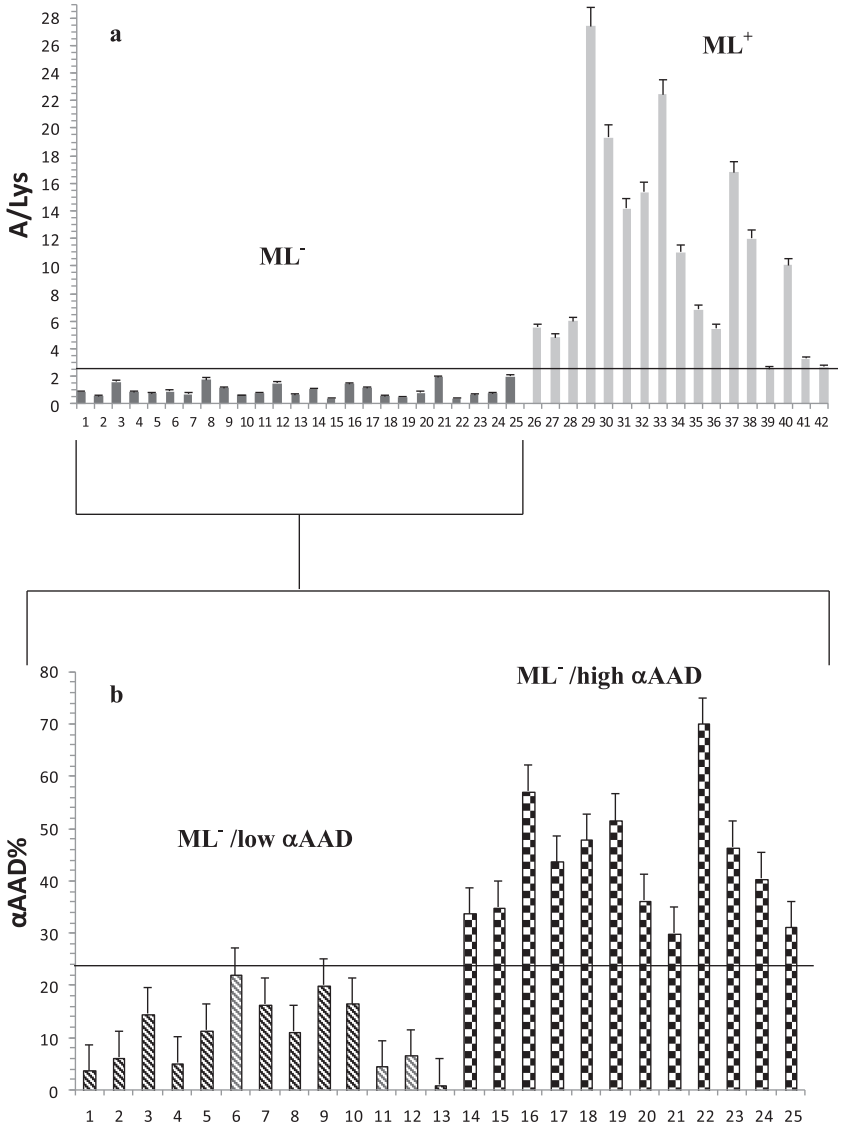

Figure 5. (a) Distribution of ML signal intensity monitored through the intensity ratio of cross peak A from ML over Lys in 42 GSC lines during exponential growth. ML^+ indicates the group of 17 lines (light grey) with intensity ratio higher than 2.5 and ML^- the group of 25 lines (dark grey) with intensity ratio lower than 2.0. Data are mean values with SD of at least three independent measurements. (b) Distribution of αAAD signal intensity in the 25 GSC lines of the ML^- group. The intensity ratio αAAD/(αAAD + Lys) that gives the percentage of catabolized Lys was monitored. The line indicates the median of this ratio in the 25 lines. Lines of the subgroup ML^-/low αAAD are indicated with stripes and those of the subgroup ML^-/high αAAD with squares. Data are mean values with SD of at least three independent measurements.

Copyright © 2015 John Wiley & Sons, Ltd.

butyric acid (GABA) has a triplet at 2.30 ppm with the cross peaks at 2.30–1.92 ppm and 3.00–1.92 ppm; ML have the C2 in fatty acid chains resonating at 2.22 ppm but the cross peak is at 1.58–2.22 ppm. αAAD signals were not found in the spectra of the corresponding GSC conditioned media.

The αAAD in GSCs is from the mitochondrial saccharopine pathway

Lys catabolism may proceed by the saccharopine and pipecolate pathways. The mitochondrial saccharopine pathway is predominant in the developing brain, while the cytoplasmatic pipecolate route prevails in the adult brain (5). In order to gain more information on the Lys degradative pathway in GSCs, a cell line with intense αAAD signals, namely line 163, was treated with the mitochondrial ATPase inhibitor oligomycin. Treated cells were arrested in proliferation at days 1–2 and subsequently died (Fig. 3(a)). Accelerated glycolysis rate was indicated by the percentage gains of lactate secretion into the culture medium at day 1–2 (not shown). αAAD signals disappeared and new signals (S) from saccharopine were found in both 1D and 2D spectra (Fig. 3(b), (c), (f), (g) and Fig. S1). The assignment of the new signals to saccharopine in treated samples was performed according to the human metabolome database (25) (Fig. S1 and Table S1 in Fig. S1). The cross peak of Lys at 1.70–3.01 ppm in 2D spectra of the control sample is almost buried under the signal at 1.76–3.05 ppm from saccharopine in oligomycin treated samples, as shown by the three-dimensional representation of the cross peaks (Fig. S1(g), (h)). Concurrently, signals from ML increased in treated samples, as seen in the 2D spectra shown in Figure 3(f), (g) (peaks A and F from ML) and confirmed by 1D spectra (Fig. 3(d), (e)).

The ML increase in oligomycin treated cells may be associated with the induced mitochondrial impairment, most likely due to inhibition of fatty acid β-oxidation, in agreement with recent literature data (26).

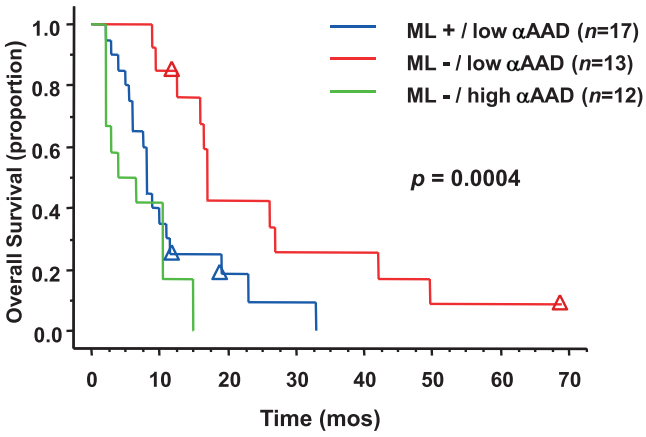

Figure 6. Kaplan–Meier plot of patients' OS. Survival differed significantly according to the presence of intense ML (group ML^+), intense AAD (ML^-/αAAD high) and low αAAD (ML^-/αAAD low) in GSCs.

αAAD is not detectable in cells with intense ML signals

αAAD signal intensities were not constant during cell growth, remaining unchanged in the first eight days in culture, while declining afterwards. In parallel, the intensity of ML signals increased. GABA signals also increased when present. Figure 4 (A)(a)–(d) shows this behavior in 1D spectra of line 23 run at day 4 and at day 11 after seeding.

In the high ML subset of cells, αAAD signals were undetectable as early as day 4 after seeding, as shown in Figure 4(B)(a)–(c).

For both lines, low or absent αAAD signals in GSC spectra with intense ML were paralleled by low/absent αAAD signals in the corresponding PCA extracts (Fig. S2(A), (B)), thus indicating that failure to detect αAAD in these samples was due not to partial overlapping of αAAD signals with the very intense signals from ML, but more likely to coupled metabolic pathways.

On these grounds, αAAD production was not monitored in GSC spectra characterized by high ML.

Intensity of αAAD signals in GSC spectra correlates with poor patient survival

Analysis of ^{1}H NMR spectra from each GSC line, repeated on different days during exponential growth, revealed that 17/42 GSCs were characterized by consistently high ML signals (A/Lys ratio > 2.5), whereas 25/42 GSCs had low/absent ML signals (A/Lys < 2) (Fig. 5(a), where the two groups are indicated as ML^+ and ML^-). Low ML levels were often found in GSCs forming larger neurospheres, despite reduced oxygen availability, which usually increases ML signals, as observed in cancer cell spheroids (19). The trend of ML increase was always observed while approaching cell confluence, though at different intensities in different GSC lines, and was accompanied by GPC increase, in agreement with previous data (19).

Taking into account the considerations of the previous paragraph, the group ML^+ of 17/42 lines was not used for αAAD evaluation. In the group of 25 ML^- lines, the intensity of αAAD signal was scored as low/absent or intense, with a threshold determined by the median value of the ML^- group (Fig. 5(b)).

Therefore, three different groups of GSCs were identified according to the measured ML and αAAD levels: ML^+ group (17 GSC lines), ML^-/$αAAD^+$ group (12 GSC lines), and ML^-/$αAAD^-$ group (13 GSC lines). A close relationship was found

Table 3. Results of multivariate analysis for patients' survival

	DF	Coeff.	Std error	Coeff./SE	Chi-square	*P*-value	Exp (coeff.)
Age	1	0.771	0.413	1.869	3.494	0.0616	2.162
KPS	1	−0.363	0.413	−0.880	0.774	0.3790	0.696
Total removal	1	0.475	0.435	1.092	1.192	0.2749	1.608
MGMT	1	−0.987	0.414	−2.385	5.688	0.0171	0.373
Mobile lipids	1	−0.677	0.449	−1.508	2.273	0.1317	0.508
Adipate	1	1.264	0.530	2.385	5.689	0.0171	3.539

Copyright © 2015 John Wiley & Sons, Ltd.

between the αAAD content in the GSCs and the overall survival (OS) of the parent patients (Fig. 6). The worst prognosis was associated with absent MLs and high αAAD content in GSC spectra ($p = 0.0004$; log rank test). It should be pointed out that, in this cohort of patients, clinical and molecular factors that are known to be predictive for OS did show prognostic value, thus validating the statistical representativeness of our sample. In fact, univariate analysis showed that age > 70 years, Karnofsky performance status (KPS) < 70, and absence of MGMT methylation were significantly associated with poor OS ($p = 0.0137$, $p = 0.0057$, and $p = 0.0025$, respectively; log rank test; Table 1 and Fig. S3).

On multivariate analysis, MGMT promoter methylation status and αAAD content emerged as independent factors that significantly affected OS ($p = 0.0171$ and $p = 0.0171$, respectively; Cox proportional hazard test; Table 3), whereas age and ML showed a trend towards significance ($p = 0.0616$ and $p = 0.1317$, respectively; Cox proportional hazard test; Fig. S3).

DISCUSSION

In the present study, an unusually high concentration of αAAD has unambiguously been ascertained in a subset of GSCs on the basis of NMR signal patterns of 1D and 2D COSY spectra. In these lines, the saccharopine mitochondrial pathway has been demonstrated as the main Lys pathway by the appearance of saccharopine signals after mitochondrial impairment with oligomycin. The saccharopine pathway is a major degradative pathway for Lys in developing brain (5). The presence of this pathway in GSCs may suggest a fetal-like metabolism, possibly bound to multipotency.

L-Lys is present in culture media and its degradative pathway produces L-αAAD. L-αAAD toxicity was proven with respect to glia and neurons, though some studies claimed a preferential toxicity towards astrocytes (27). Paradoxically, the presence of the "gliotoxin" does not affect tumor cell growth as the tumor recurs, resulting in very short patient survival, as here observed in the αAAD positive group of cells. αAAD is normally excreted in urine at nanomolar concentrations (6,28), while abnormal levels are present in urine and plasma (where it is normally absent) in the human disease known as aminoadipicaciduria (see case reports in References 28 and 29). Although a direct hypothesis on the disease origin is not available, current literature attributes the neurological symptoms to αAAD gliotoxic properties.

The dramatic increase of the αAAD molecule in GSCs together with the observation that its signals were not detectable in ^{1}H spectra of OB-NPCs and of HNPC point to a role of αAAD as a cancer biomarker. αAAD is the product of the α-aminoadipic semialdehyde–ALDH7A1 complex. ALDH7A1, present in mitochondria, in cytoplasm and even in the nucleus in different cells (30), exerts its protective function during oxidative stress along with a significant increase in cell survival (31). Our data would indicate that in GSCs this protective function is predominantly performed in mitochondria, where αAAD formation is located.

The high levels of αAAD found in GSCs are difficult to explain, as different pathways may lead to the same result. In fact, abnormal αAAD concentration may be originated by ALDH7A1 upregulation, by a downregulation of 2-aminoadipate aminotransferase (2-AAT) (the enzyme responsible for the catalysis of the reversible transamination of 2-AAD and 2-oxoglutarate to form 2-oxoadipate and glutamate) or by a decrease of the substrate 2-oxoglutarate as found in other gliomas of lower degree (32).

Statistical analysis has shown here that αAAD signal intensity is an independent predictive factor of survival. The observed unusually high intensity of αAAD concentration could be related to increased enzymatic activity of ALDH7A1, as previous studies have shown that ALDH7A1 is highly expressed in human prostate cancer cells and in clinical specimens of primary prostate tumors with matched bone metastases (33,34). Furthermore, low ALDH7A1 expression was associated with decreased cancer recurrence in patients with non-small-cell lung carcinomas (35).

Nevertheless, the impairment of the successive steps of Lys catabolism after αAAD production, that is downregulation of 2-AAT or decrease of the substrate 2-oxoglutarate, cannot be ruled out. Impairment of the successive steps of Lys catabolism after αAAD production seems unlikely in the examined GSCs. In fact, Lys is a ketogenic aminoacid and its degradation goes into final steps that include fatty acid synthesis instead of providing substrates for mitochondria, as also indicated by recent literature (12,36). On the basis of the inverse correlation observed for αAAD and ML signals, lipid synthesis does not seem hindered in GSCs, suggesting the involvement of αAAD in processes successive to its formation. Specific studies are necessary to analyze these hypotheses.

A previous study on surgical glioma tissues included αAAD in the metabolites observed in Grade IV glioma, although the concentrations were not given (13 – supplementary section). In the study by Chinnaiyan *et al*., Grade IV glioma patients were divided into two subgroups according to the prevailing metabolism in their tumors. The shortest survival was associated with the phospholipid catabolism group, the remaining patients being associated with a purely anabolic metabolism. In the present study, shorter patient survivals were associated with GSCs with either lipid metabolism (subgroup ML^+) or high αAAD level (subgroup $ML^-/\alpha AAD^+$). The presence of subgroups of GSCs characterized by different ML intensities is in agreement with the shortest survival of the phospholipid catabolism subgroup observed in GBM by Chinnaiyan *et al*. (13). Many studies have been conducted on the role of neutral lipids and the balance of FA anabolism and catabolism in cancer and in stem cells, yet a clear picture is not at hand and this topic deserves further studies.

In conclusion, αAAD levels measured in the GSCs examined here correlated with tumor aggressiveness, independent of other markers. αAAD levels together with gene analysis or protein expression may therefore be explored to provide independent determinant prognostic factors in GBM and may help in creating comprehensive risk models incorporating both molecular and metabolic markers.

Acknowledgements

This work was supported by the INFN project RADIOSTEM and by a grant from Associazione Italiana per la Ricerca sul Cancro, AIRC (start-up 6326 to LRV).

REFERENCES

1. Smith JS, Jenkins RB. Genetic alterations in adult diffuse glioma: occurrence, significance, and prognostic implications. Front. Biosci. 2000; 5: D213–231.

 Copyright © 2015 John Wiley & Sons, Ltd.

2. Jackson B, Brocker C, Thompson DC, Black W, Vasiliou K, Nebert DW, Vasilou V. Update on the aldehyde dehydrogenase gene (ALDH) superfamily. Hum. Genomics 2011; 5: 283–303.
3. Allahverdiyev AM, Bagirova M, Oztel ON, Yaman S, Abamor ES, Koc RC, Ates SZ Elcicek S, Baydar SY. In *Aldehyde Dehydrogenase: Cancer and Stem Cells, Dehydrogenases*, Canuto RA (ed.). InTech, 2012; 3–26.
4. Jackson B, Brocker C, Thompson DC, Black W, Vasiliou K, Nebert DW, Vasiliou V. Update on the aldehyde dehydrogenase gene (ALDH) superfamily. Hum. Genomics 2011; 5(4): 283–303.
5. Hallen A, Jamie JF, Cooper AJL. Lysine metabolism in mammalian brain: an update on the importance of recent discoveries. Amino Acids 2013; 45: 1249–1272.
6. Guidetti P, Schwarcz R. Determination of α-aminoadipic acid in brain, peripheral tissues and body fluids using GC/MS with negative chemical ionization. Mol. Brain Res. 2003; 118: 132–139.
7. Gerrits GP, Trijbels FJ, Monnens LA, Gabreëls FJ, De Abreu RA, Theeuwes AG, van Raay-Selten B. Reference values for amino acids in cerebrospinal fluid of children determined using ion-exchange chromatography with fluorimetric detection. Clin. Chim. Acta 1989; 182: 271–280.
8. Oepen G, Cramer H, Bernasconi R, Martin P. Huntington's. Disease-imbalance of free amino acids in the cerebrospinal fluid of patients and offspring at-risk. Arch. Psychiatr. Nervenkrankh. 1982; 231: 131–140.
9. Griffin JL, Kauppinen RA. A metabolomics perspective of human brain tumours. FEBS J. 2007; 274: 1132–1139.
10. Mlynarik V, Cudalbu C, Xin L, Gruetter R. ^{1}H NMR spectroscopy of rat brain *in vivo* at 14.1 Tesla: improvements in quantification of the neurochemical profile. J. Magn. Reson. 2008; 194: 163–168.
11. Locasale JW, Melman T, Song S, Yang X, Swanson KD, Cantley LC, Wong ET, Asara JM. Metabolomics profiling of patient cerebrospinal fluid identifies signatures of malignant glioma. Mol. Cell. Proteomics 2012; 11: 1–12.
12. Bellance N, Pabst L, Allen G, Rossignol R, Nagrath D. Oncosecretomics coupled to bioenergetics identifies α-amino adipic acid, isoleucine and GABA as potential biomarkers of cancer: differential expression of c-Myc, Oct1 and KLF4 coordinates metabolic changes. Biochim. Biophys. Acta 2012; 1817: 2060–2071.
13. Chinnaiyan P, Kensicki E, Bloom G, Prabhu A, Sarcar B, Kahali S, Eschrich S, Qu X, Forsyth P, Gillies R. The metabolomic signature of malignant glioma reflects accelerated anabolic metabolism. Cancer Res. 2012; 72(22): 5878–5888.
14. Pallini R, Ricci-Vitiani L, Banna GL, Signore M, Lombardi D, Todaro M, Stassi G, Martini M, Maira G, Larocca LM, De Maria R. Cancer stem cell analysis and clinical outcome in patients with glioblastoma multiforme. Clin. Cancer Res. 2008; 14: 8205–8212.
15. Ricci-Vitiani L, Pallini R, Larocca LM, Lombardi DG, Signore M, Pierconti F, Petrucci G, Montano N, Maira G, De Maria R. Mesenchymal differentiation of glioblastoma stem cells. Cell Death Differ. 2008; 15: 1491–1498.
16. Ricci-Vitiani L, Pedini F, Mollinari C, Condorelli G, Bonci D, Bez A, Colombo A, Parati E, Peschle C, De Maria R. Absence of caspase 8 and high expression of PED protect primitive neural cells from cell death. J. Exp. Med. 2004; 200: 1257–1266.
17. Casalbore P, Budoni M, Ricci-Vitiani L, Cenciarelli C, Petrucci G, Milazzo L Montano N, Tabolacci E, Maira G, Larocca LM, Pallini R. Tumorigenic potential of olfactory bulb-derived human adult neural stem cells associates with activation of TERT and NOTCH1. PLoS One 2009; 4(2): e4434.
18. Palma A, Grande S, Rosi A, Luciani AM, Guidoni L, Viti V. ^{1}H MRS can detect aberrant glycosylation in tumour cells a study of the HeLa cell line. NMR Biomed. 2010; 24: 1099–1110.
19. Guidoni L, Ricci-Vitiani L, Rosi A, Palma A, Grande S, Luciani AM, Pelacchi F, di Martino S, Colosimo C, Biffoni M, De Maria R, Pallini R, Viti V. ^{1}H NMR detects different metabolic profiles in glioblastoma stem-like cells. NMR Biomed. 2014; 27: 129–145.
20. Binesh N, Yue K, Fairbanks L, Thomas MA. Reproducibility of localized 2D correlated MR spectroscopy. Magn. Reson. Med. 2002; 48: 942–948.
21. Barba I, Cabanas ME, Arus C. The relationship between nuclear magnetic resonance-visible lipids, lipid droplets, and cell proliferation in cultured C6 cells. Cancer Res. 1999; 59: 1861–1868.
22. Luciani A, Grande S, Palma A, Rosi A, Giovannini C, Sapora O, Viti V, Guidoni L. Characterization of ^{1}H NMR detectable mobile lipids in cells from human adenocarcinomas. FEBS J. 2009; 276: 1333–1346.
23. Ramm P, Couillard-Despres S, Plötz S, Rivera FJ, Krampert M, Lehner B, Kremer W, Bogdahn U, Kalbitzer HR, Aigner L. Nuclear magnetic resonance biomarker for neural progenitor cells: is it all neurogenesis? Stem Cells 2009; 27: 420–423.
24. Nicholls AW, Holmes E, Lindon JC, Shockcor JP, Farrant RD, Haselden JN, Damment SJ, Waterfield CJ, Nicholson JK. Metabonomic investigations into hydrazine toxicity in the rat. Chem. Res. Toxicol. 2001; 14: 975–987.
25. HMDB database. http://www.hmdb.ca/.
26. Boren J, Brindle KM. Apoptosis-induced mitochondrial dysfunction causes cytoplasmic lipid droplet formation. Cell Death Differ. 2012; 19(9): 1561–1570.
27. Khurgel M, Koo AC, Ivy G. Selective ablation of astrocytes by intracerebral injections of α-aminoadipate. Glia 1996; 16: 351–358.
28. Lee JS, Hoon HR, Coen CJ. A Korean girl with α-aminoadipic and α-ketoadipicaciduria accompanied with elevation of hydroxyglutarate and glutarate. J. Inherit. Metab. Dis. 2001; 24: 509–510.
29. Casey RE, Zaleski WA, Philp M, Mendelson IS, MacKenzie SL. Biochemical and clinical studies of a new case of alpha-aminoadipicaciduria. J. Inherit. Metab. Dis. 1978; 1: 129–135.
30. Wong JW, Chan C, Tang W, Cheng CH, Fong W. Is antiquitin a mitochondrial enzyme? J. Cell. Biochem. 2010; 109: 74–81.
31. Brocker C, Cantore M, Failli P, Vasiliou V. Aldehyde dehydrogenase 7A1 (ALDH7A1) attenuates reactive aldehyde and oxidative stress induced cytotoxicity. Chem. Biol. Interact. 2011; 191: 269–277.
32. Dang L, White DW, Gross S, Bennett BD, Bittinger MA, Driggers EM, Fantin VR, Jang HG, Jin S, Keenan MC, Marks KM, Prins RM, Ward PS, Yen KE, Liau LM, Rabinowitz JD, Cantley LC, Thompson CB, Vander Heiden MG, Su SM. Cancer-associated IDH1 mutations produce 2-hydroxyglutarate. Nature 2009; 462: 739–744.
33. van den Hoogen C, van der Horst G, Cheung H, Buijs JT, Lippitt JM, Guzmán-Ramírez N, Handy FC, Eaton CL, Thalmann GN, Cecchini MG, Pelger RC, van der Pluijm G. High aldehyde dehydrogenase activity identifies tumor-initiating and metastasis-initiating cells in human prostate cancer. Cancer Res. 2010; 70: 5163–5173.
34. van den Hoogen C, van der Horst G, Cheung H, Buijs JT, Pelger RCM, van der Pluijm G. The aldehyde dehydrogenase enzyme 7A1 is functionally involved in prostate cancer bone metastasis. Clin. Exp. Metastasis 2011; 28: 615–625.
35. Giacalone NJ, Den RB, Eisenberg R, Chen H, Olson SJ, Massion PP, Carbone DP, Lu B. ALDH7A1 expression is associated with recurrence in patients with surgically resected non-small-cell lung carcinoma. Future Oncol. 2013; 9: 737–745.
36. Çakir T, Alsan S, Saybaşili H, Akin A, Ülgen KÖ. Reconstruction and flux analysis of coupling between metabolic pathways of astrocytes and neurons: application to cerebral hypoxia. Theor. Biol. Med. Modelling 2007; 4 (48): 1–18.

SUPPORTING INFORMATION

Additional supporting information may be found in the online version of this article at the publisher's web site.

Copyright © 2015 John Wiley & Sons, Ltd.